https://doi.org/10.5194/egusphere-2026-4284
Preprint. Discussion started: 15 September 2026

Detecting glacier-scale mass-balance heterogeneity using ASTER DEM differencing

Mariia Usoltseva[1], Roland Pail[1], Christoph Mayer[2], Martin Rückamp[2], and Anja Wendt[2]

[1]Chair of Astronomical and Physical Geodesy, Technical University of Munich, Munich, Germany
[2]Geodesy and Glaciology, Bavarian Academy of Sciences and Humanities, Munich, Germany

Correspondence: Mariia Usoltseva (mariia.usoltseva@tum.de)

Abstract. Glaciers in the Southern Andes show substantial spatial variability in mass balance, reflecting the combined effects of spatial variations in climate forcing and differences in glacier geometry. This study analyses elevation change patterns and climatic drivers for two contrasting glacier systems in southern Chile: the Queulat Glacier Complex and the stratovolcano Melimoyu. Elevation changes from 2000 to 2026 were derived from multi-temporal digital elevation models and analysed using a hypsometric approach to resolve elevation-dependent mass balance.

The results present a pronounced contrast between the two glacier systems. The Queulat Glacier Complex experiences consistently negative mass balance throughout the study period, with a rate of mass loss increasing from approximately -0.23 ± 0.39 to -0.63 ± 0.19 m w.e./yr. In contrast, Melimoyu maintained positive or near-balanced conditions in the early 2000s, followed by a transition to slightly negative mass balance in recent years. Elevation-dependent analyses show that mass loss in Queulat is predominantly associated with extensive low-elevation glacier tongues, while Melimoyu is characterised by a top-heavy hypsometry with a large accumulation area at high elevations.

Examination of downscaled ERA5 reanalysis data shows a consistent regional warming and a decrease in solid precipitation over the study period, while differences in total precipitation between the two sites remain small. This suggests that the contrasting glacier behaviour is not primarily driven by differences in climatic forcing, but rather by differences in glacier geometry and elevation distribution, which modulate the sensitivity to warming.

These results underline the key role of hypsometry and spatial glacier structure in determining individual glacier responses to climate change. The study indicates that glaciers under similar climatic conditions can exhibit substantially different mass-balance trajectories due to their geometry.

1 Introduction

Satellite-based geodetic methods have transformed the quantification of glacier mass change at regional to global scales, enabling robust estimates of long-term trends and glacier contributions to sea-level rise. Studies based on multi-sensor Digital Elevation Model (DEM) differencing, satellite altimetry, gravimetry and sensor fusion now offer near-global coverage and internally consistent regional and global mass-balance estimates (e.g., Wouters et al., 2019; Dussaillant et al., 2019; Brun et al., 2017; Hugonnet et al., 2021; Chen et al., 2006; Moholdt et al., 2010). However, these large-scale datasets inherently rely on

https://doi.org/10.5194/egusphere-2026-4284
Preprint. Discussion started: 15 September 2026

spatial averaging and methodological generalisation, which can suppress glacier-scale variability in elevation changes and mass balance (Zemp et al., 2019; Huss and Hock, 2015; McDonnell et al., 2022).

The Southern Andes constitute one of the largest glacierized regions outside the polar regions and are among the most important contributors to contemporary global glacier mass loss (Hugonnet et al., 2021; Dussaillant et al., 2019). Within Patagonia, glacier change exhibits pronounced spatial variability despite experiencing broadly similar regional climatic conditions (Van Wyk de Vries et al., 2023; Rivera and Bown, 2013; Malz et al., 2018). Previous studies have documented widespread glacier retreat, thinning and mass loss throughout the northern Patagonian region (Rivera and Bown, 2013; Willis et al., 2012a; Dussaillant et al., 2019), but also substantial differences among neighbouring glaciers that cannot be explained by climate alone (Malz et al., 2018; Braun et al., 2019). These observations suggest that local controls, including glacier geometry, elevation distribution and dynamic regime, play an important role in modulating glacier response to climate variability and change (Huss, 2012; Paul, 2015; Braun et al., 2019).

This glacier-scale variability is particularly relevant in northern Patagonia, where outlet-glacier systems, volcanic ice caps and mountain glaciers coexist within the same climatic setting but exhibit markedly different geometries and dynamic behaviour. Understanding this spatial heterogeneity is essential for hydrological applications, model calibration, and the downscaling of regional estimates to individual glaciers (Hock et al., 2019).

To better quantify glacier-scale variability, observations that resolve individual glacier behaviour are required. However, the capacity of widely used satellite DEMs to capture glacier-specific mass-change signals varies considerably. Sensor limitations, data gaps, and measurement noise introduce bias into elevation-change estimates, particularly for small or morphologically complex glaciers (Brun et al., 2017; Berthier et al., 2016). Although DEM differencing products are widely used, the extent to which glacier geometry influences the detectability and interpretation of mass-change signals remains insufficiently quantified. This challenge is particularly relevant in the Southern Andes, where substantial discrepancies persist among mass-balance estimates derived from different observational methods, as highlighted by The GlaMBIE Team et al. (2025). This inter-method variability further highlights the need to better understand how methodological choices and glacier morphology influence the estimates of glacier mass change.

This study investigates these questions through ASTER-derived DEM differencing for two neighbouring Patagonian glaciers exhibiting contrasting geomorphology: a low-gradient glacier complex with classical outlet glaciers and a steep, volcano-influenced glacier. By quantifying elevation-change rates over multiple time intervals and across elevation bands,we examine how differences in glacier hypsometry, elevation range, and area-elevation distribution influence thinning patterns and glacier sensitivity to shifts in equilibrium-line altitude, assess the detectability of accumulation and thinning signals using ASTER data, and evaluate the implications for downscaling regional mass-change estimates to the glacier scale.

https://doi.org/10.5194/egusphere-2026-4284
Preprint. Discussion started: 15 September 2026

2 Data and Study Area

2.1 Test sites

We selected a sub-region located within the northern sector of Chilean Patagonia, immediately north of the Northern Patagonian Ice Field (Figure 1 a)), characterised by several large glaciers within a relatively confined area. This region corresponds to the Wet Andes subregion, which is known for a humid temperate climate strongly influenced by the Southern Westerlies, resulting in high annual precipitation totals and extensive glacierization on the western slopes of the Andes (Garreaud, 2009). Additionally, this region is highly subject to inter-annual temperature and precipitation variability due to the impact of ENSO (Garreaud et al., 2009). Glaciers in this region have experienced widespread retreat and mass loss during recent decades, consistent with observations across much of Patagonia (Dussaillant et al., 2019; Malz et al., 2018). However, considerable variability in glacier response has been observed at local scales, highlighting the importance of glacier-specific controls.

The study region spans approximately 110 × 80 km (1° × 1°). The choice of this location is justified by the proximity of two relatively large glacier complexes (GC) with very different geometries, which allows the investigation of spatial heterogeneity in glacier mass change under comparable climatic conditions. Within this sub-region, two GCs were selected for detailed analysis. The first is the Queulat GC, which covers an area of approximately 102 km^2 and comprises several glaciers, including two major outlet glaciers (Figure 1, c)). The second site is the ice-covered stratovolcano Melimoyu, with a glacierized area of approximately 55 km^2 (Figure 1, d)).

Both GCs exhibit comparable elevation ranges: Queulat spans approximately 600 to 2100 m a.s.l., and Melimoyu spans approximately 600 to 2500 m a.s.l. Their close spatial proximity (about 50 km linear distance) and similar elevation ranges suggest that both systems are subjected to similar large-scale climatic forcing. At the same time, the two sites differ substantially in their geomorphology and glacier structure. Queulat represents a complex glacier system with two large outlet glaciers and a large proportion of glacier area concentrated within a relatively narrow elevation range between 1400 and 1800 m a.s.l.. In contrast, Melimoyu is a steep volcanic ice cap with few minor glacier tongues and glacier area distributed over a larger elevation range. This contrast provides an opportunity to assess how glacier geometry influences observed elevation-change patterns and to evaluate the ability of ASTER-derived DEMs to resolve these differences.

The contrasting hypsometries of the two glacier complexes are of particular interest because the distribution of glacier area with elevation is known to influence glacier sensitivity to equilibrium-line altitude fluctuations and climatic change (Huss, 2012; Paul, 2015). Glaciers with large areas concentrated within a limited elevation range may exhibit strong responses to relatively small shifts in the equilibrium-line altitude, whereas glaciers spanning a broader elevation range may retain accumulation areas under similar climatic conditions.

2.2 ASTER DEMs

DEMs used in this study were acquired by the Advanced Spaceborne Thermal Emission and Reflection Radiometer (ASTER) onboard the Terra satellite. Terra is a multi-national Earth observation satellite operating in a sun-synchronous orbit with a 16-day repeat cycle and has been providing data since its launch in December 1999 (NASA JPL, 2004).

https://doi.org/10.5194/egusphere-2026-4284
Preprint. Discussion started: 15 September 2026

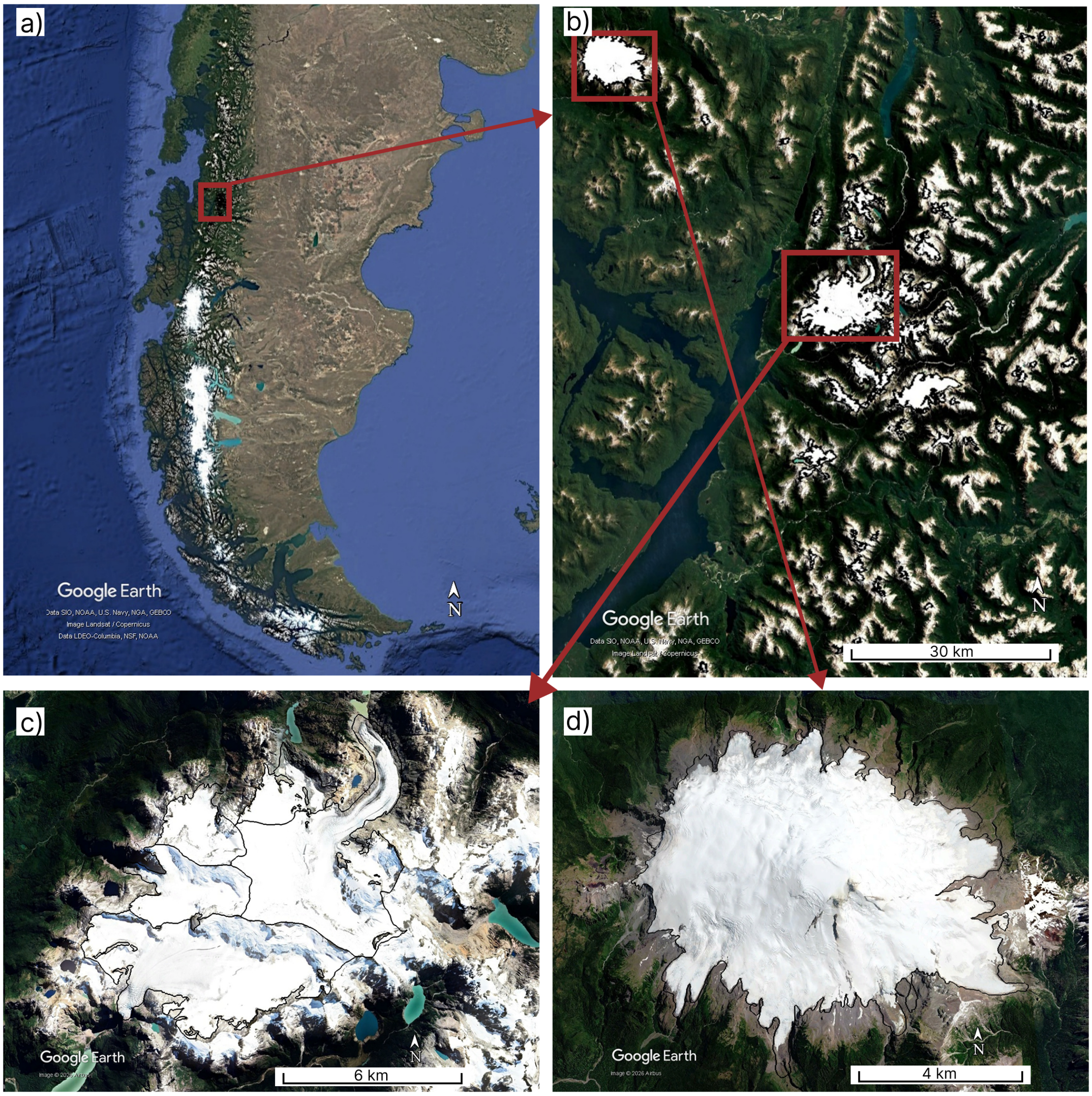

Figure 1. Google Earth images of study sites: location of area of interest in South America a), area of interest b), Queulat GC c) and stratovolcano Melimoyu d). Maps data: ©Google Earth 2026 a) Image Landsat/Copernicus, Data LDEO-Columbia, NSF, NOAA, b) Image Landsat/Copernicus, Data LDEO-Columbia, NSF, NOAA c) Image: ©Airbus, 2025, d) Image: ©Airbus, 2026

ASTER DEMs are generated using along-track stereoscopy in the visible and near-infrared (VNIR) spectral range. The VNIR subsystem is equipped with two telescopes: a nadir-viewing sensor (3N) and a backwards-looking sensor (3B), separated by an angle of approximately 27.6° (Abrams, 2000). These sensors almost simultaneously acquire stereo image pairs of terrain from different viewing geometries. Then, elevation information is derived by measuring the parallax (displacement) between corresponding features in the stereoscopic image pair. This difference is converted into surface elevation through pho-

https://doi.org/10.5194/egusphere-2026-4284
Preprint. Discussion started: 15 September 2026

togrammetric processing using known sensor geometry, orbit parameters, and image orientation models (Fujisada et al., 2005). The resulting DEMs typically have a spatial resolution of 15–30 m and are widely used for regional to global topographic analysis.

In this study, we use the AST14DEM product (NASA et al., 2025) generated by NASA from ASTER Level 1A data. The resulting DEMs have a 30 m spatial resolution and are derived from a single stereo image pair acquired on the same date. This characteristic provides a well-defined acquisition timestamp, which is particularly advantageous for DEM differencing applications.

Seasonal variations in snow cover can introduce biases in DEM differencing; therefore, end-of-ablation-season acquisitions are generally preferred. To mitigate the seasonal effects, we utilise only DEMs acquired during the hydrological summer (October 1 to March 31 for the southern hemisphere).

2.3 Reference DEM

Accurate co-registration of ASTER DEMs requires a stable and high-quality reference DEM to minimise systematic elevation biases and spatial offsets. For this purpose, the SRTM DEM is commonly used in glacier studies due to its near-global coverage and relatively consistent quality (e.g., Willis et al., 2012b; Berthier et al., 2016). DEMs used for the SRTM global DEM were taken by the SRTM instrument aboard the Space Shuttle Endeavour between 11 and 22 February, 2000 (NASA Earthdata). However, the original SRTM DEM contains voids and artefacts, particularly in regions of steep and complex terrain, arising from geometric distortions and limitations of the radar acquisition system.

Here, we use the NASADEM product, a void-filled global one-arcsecond (30 m) DEM derived from reprocessed SRTM data (NASA JPL, 2020). The higher spatial resolution of NASADEM is particularly beneficial for studies in complex mountainous terrain, as it allows for a more detailed representation of topography compared to 3 arc-second (90 m) SRTM Void-Filled product. NASADEM incorporates improvements over the original SRTM product, including enhanced phase unwrapping algorithms and corrections of elevation artefacts such as residual height ripples (Buckley et al., 2025). These updates result in improved spatial consistency and reduced systematic errors, making NASADEM a more suitable reference surface for DEM co-registration.

2.4 Glacier complex and water bodies outlines

For co-registration purposes, it is essential to distinguish between stable and unstable terrain. To classify areas within the DEM accordingly, we mask out glacierized regions and water bodies, which are considered unstable surfaces.

Glacier outlines are obtained from the Randolph Glacier Inventory version 7 (RGI 7) (RGI 7.0 Consortium, 2023). The RGI is a globally complete inventory of glacier outlines compiled by the Global Land Ice Measurements from Space (GLIMS) initiative. In this study, we use the glacier complex product, which represents contiguous ice masses by merging individual glaciers that share common boundaries into unified GCs.

Water bodies are identified using the Global Lakes and Wetlands Database version 2 (GLWD) (Lehner et al., 2025). GLWD provides a comprehensive and seamless global map of inland surface waters, distinguishing 33 classes of lakes, reservoirs,

https://doi.org/10.5194/egusphere-2026-4284
Preprint. Discussion started: 15 September 2026

rivers, and wetland types. In this study, GLWD is used to mask water bodies, which are considered unstable surfaces for DEM co-registration. Excluding these areas helps to prevent biases arising from temporal variability in water levels and surface properties.

2.5 ERA5

To estimate local temperature and precipitation changes in the sub-region of interest and investigate their relationship with elevation change trends derived from DEM differencing, we use ERA5 reanalysis data for temperature and precipitation. Hourly data for the *2 meter Temperature* and *Total precipitation* were obtained for the period from 2000 to 2026 (Copernicus Climate Change Service, 2023).

ERA5 is a state-of-the-art atmospheric reanalysis product generated using data assimilation techniques, in which a numerical weather prediction model is continuously constrained by a wide range of observations, including weather stations and satellites. This approach combines model forecasts with observations to produce a physically consistent and temporally complete estimate of atmospheric and surface conditions. As a result, ERA5 provides a comprehensive and internally consistent representation of the global atmosphere, land surface, and ocean waves (Hersbach et al., 2020).

3 Methods

The DEM processing workflow used in this study is summarised in Figure 2. The workflow consists of preprocessing steps aimed at filtering outliers and aligning all DEMs to a common reference frame, followed by processing steps to derive spatially distributed elevation-change rates and their elevation-dependent patterns, as well as glacier mass balance (GMB). Detailed descriptions of each processing step are provided in the subsections below.

3.1 DEM pre-processing

The DEM pre-processing workflow applied in this study follows established approaches commonly used in glacier elevation change studies based on DEM differencing.

The AST14DEM V004 product, unlike the earlier V003 version, does not include cloud coverage in its metadata. To identify and remove cloud-contaminated pixels, we compute the elevation difference between each ASTER DEM and the reference NASADEM. Pixels with absolute elevation differences exceeding 300 m are assumed to be affected by clouds and are masked.

For co-registration, ASTER DEMs are aligned to the common reference DEM (NASADEM) using the universal co-registration method (Nuth and Kääb, 2011) implemented in xDEM package (xDEM contributors, 2026). This method is based on minimising horizontal and vertical offsets by exploiting the relationship between elevation differences and terrain attributes (slope and aspect), solving a cosine-based model of elevation bias.

Following coregistration, a three-step threshold-based outlier filtering is applied:

1. **Physically based elevation change threshold.** The threshold is based on the assumption of maximal plausible melt and accumulation per year. Pixels are retained only if their elevation differences relative to the reference DEM fall within a range

https://doi.org/10.5194/egusphere-2026-4284
Preprint. Discussion started: 15 September 2026

of -20 m/yr to +15 m/yr. Values outside this range are considered unrealistic and are removed. The upper threshold (+15 m/yr) is constrained by the assumption that net accumulation cannot exceed the total annual solid precipitation. As shown in Figure 7, maximum annual solid precipitation reaches approximately 11 000 mm w.e./ yr, corresponding to roughly 13 m/yr, which is consistent with the applied upper bound. The lower threshold (-20 m yr^{-1}) was selected based on reported maximum melt rates reaching 15 m/yr for glaciers within Northern Patagonian Ice Field (Willis et al., 2012a).

2. **Temporal median filter.** For each pixel, elevation values are compared to the temporal median derived from the full DEM stack. Pixels deviating by more than 100 m from the temporal median are classified as outliers and masked. While some studies apply thresholds of 100–150 m (e.g., Brun et al., 2017; Kääb et al., 2012), a threshold of 100 m was selected here based on visual inspection of elevation-difference histograms across elevation bands, which showed that most values fall within the 0–80 m range.

3. **Three-sigma filter.** A statistical filter is applied by computing the mean and standard deviation of elevation values for each pixel across the DEM stack. Pixels are retained only if their values lie within $\pm$ 3 standard deviations of the mean. This step removes remaining outliers, including those with moderate deviations (<100 m) that are nonetheless inconsistent with the local elevation distribution.

After co-registration and outlier filtering, a stack of improved-quality DEMs is obtained. However, an additional pre-processing step is required. Although the DEMs are largely free of clouds and major outliers, they still contain residual high-frequency “salt-and-pepper” noise of small magnitude. Common smoothing approaches, such as Gaussian blurring or median filtering, can reduce this noise, but they tend to degrade sharp topographic features, particularly along ridges and steep slopes.

To address this limitation, we apply a bilateral filtering method, which reduces noise while preserving terrain edges. The bilateral filter achieves this by combining spatial proximity and radiometric similarity: pixel values are smoothed not only by their spatial distance but also by their elevation similarity (Zhang and Gunturk, 2008). As a result, the filter effectively suppresses small-scale noise while maintaining sharp discontinuities, such as mountain ridges and valley boundaries.

After applying outlier filtering and bilateral smoothing, only DEMs that meet the quality criteria are retained. Specifically, DEMs are kept if they contain more than 15% valid elevation pixels within the glaciers of interest and if the standard deviation of elevation differences relative to the reference DEM over ice-free terrain is below 20 m.

3.2 Derivation of Elevation Change and Mass Balance

To derive elevation change maps from the stack of pre-processed DEMs, we utilise a two-step pixel-wise linear regression approach, which has been widely applied in other glacier elevation change studies (e.g., Wang and Kääb, 2015; Berthier et al., 2016; Brun et al., 2017; Dussaillant et al., 2019). In the first step, the reference DEM is included in the DEM stack, and a weighted linear regression is fitted independently for each pixel. The weights are derived from the standard deviation of elevation differences over non-glacierized terrain between each AST14DEM and the reference DEM.

https://doi.org/10.5194/egusphere-2026-4284
Preprint. Discussion started: 15 September 2026

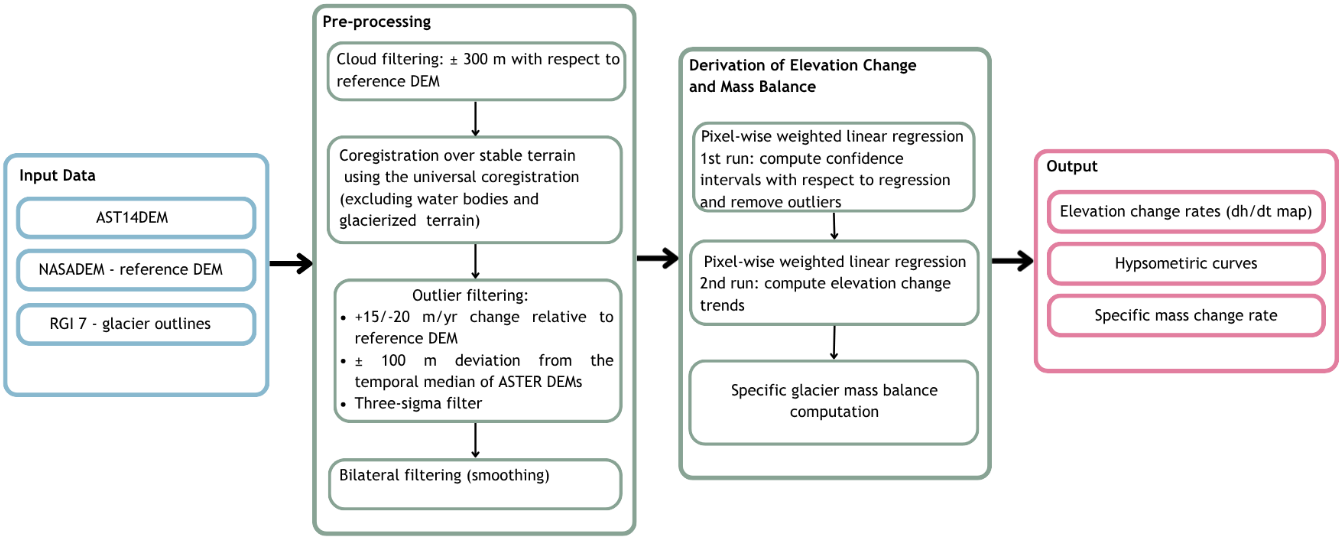

Figure 2. Schematic processing workflow

The initial regression results are used to estimate 99% confidence intervals for the elevation change trends. Observations that fall outside these confidence intervals are considered outliers and are removed. A second weighted linear regression is then performed for each pixel using the filtered dataset to obtain robust estimates of elevation change.

From the resulting elevation change maps, glacier-wide specific mass balance (GMB) is calculated using the hypsometric method to account for the distribution of elevation changes across different altitude bands of the glacier (Pop):

$$GMB = \sum_{i=1}^{n} \left(\frac{dh}{dt} \cdot S \right)_i \cdot \rho, \tag{1}$$

where *dh/dt* - mean elevation change rate per elevation band, *S*- glacier area per elevation band, ρ - volume to mass conversion factor of 850 ± 60 kg m^{-3} (Huss, 2013), n - number of elevation bands.

The analysis is conducted for two test GCs over multiple time periods to assess temporal variability in elevation change. The selected periods are 2000–2010, 2011–2015, 2016–2020, and 2021–2026. The first period spans 10 years, whereas the subsequent intervals are shorter, due to the limited availability of DEMs in the study region between 2000 and 2010.

3.3 Uncertainty analysis

For calculating uncertainty in elevation change rates, two approaches are commonly used in the literature:

https://doi.org/10.5194/egusphere-2026-4284
Preprint. Discussion started: 15 September 2026

1.The uncertainty of elevation change rates (dh/dt) can be derived directly from the linear regression applied to each pixel time series. A weighted least squares model provides both the estimated trend and its associated standard error (σ_{pixel}). By computing the quadratic mean of these pixel-wise errors, the overall uncertainty σ_{dh} can be obtained (Wang and Kääb, 2015).

2. The second approach estimates uncertainty as the standard deviation of elevation changes over stable terrain derived from the final dh/dt map. This approach does not account for spatial correlation but is considered appropriate when the area of study is larger than the decorrelation area (Fischer et al., 2015).

We computed σ_{dh} using both methods for the full study period (2000–2026). For Queulat GC, the quadratic mean of the regression-based slope error is 0.38 m, compared to 0.58 m derived from the standard deviation of elevation changes on stable terrain. For Melimoyu, the regression-based RMS is 0.30 m, whereas the stable-terrain method yields 0.42 m.

In the following, we adopt σ_{dh} derived from the standard deviation of elevation changes over stable terrain for glacier-wide elevation change estimates in order to avoid underestimating uncertainties. For elevation-band-specific uncertainties ($\sigma_{dh,\text{bin}}$), we use the quadratic mean of the regression-based slope errors computed for all pixels within each elevation bin. This approach is necessary because stable-terrain elevation distributions do not match those of glacierized areas, making the standard deviation method inapplicable at the elevation-bin scale.

Uncertainties in glacier-wide mass balance estimates were calculated following the approach of Brun et al. (2017). The total uncertainty in mass balance ($\sigma_{\Delta M,\text{tot}}$) is computed as the quadratic sum of a random component ($\sigma_{\Delta M,\text{rand}}$) and a systematic component ($\sigma_{\Delta M,\text{sys}}$):

$$\sigma_{\Delta M,\text{tot}} = \sqrt{\sigma^2_{\Delta M,\text{rand}} + \sigma^2_{\Delta M,\text{sys}}}. \quad (2)$$

The random uncertainty is assumed to originate from three independent sources: uncertainties in elevation change rates (σ_{dh}), glacier area ($\sigma_A = 10\% \cdot A_{glacier}$ (Kääb et al., 2012)), and the volume-to-mass conversion factor (σ_ρ). These contributions are combined assuming independence of errors. Assuming independence between error sources, the uncertainty in volume change is computed as:

$$\sigma_{\Delta V} = \sqrt{(\sigma_{dh} \cdot A_{glacier})^2 + (\sigma_A \cdot \Delta h)^2}, \quad (3)$$

which is then propagated to mass change using the density factor $\rho = 850$ kg/m^3 with associated uncertainty $\sigma_\rho = 60$ kg/m^3 (Huss, 2013):

$$\sigma_{\Delta M,\text{rand}} = \sqrt{(\sigma_{\Delta V} \cdot \rho)^2 + (\sigma_\rho \cdot \Delta V)^2}, \quad (4)$$

The systematic uncertainty includes biases associated with DEM differencing, quality and number of DEMS and is computed as:

$$\sigma_{\Delta M,\text{sys}} = |\Delta M_{total} - \frac{1}{2} \cdot (\Delta M_1 + \Delta M_2)\,|, \quad (5)$$

where ΔM_{total} corresponds to GMB for the total study period, ΔM_1 - GMB of first half of study period and ΔM_2 - second half of study period.

https://doi.org/10.5194/egusphere-2026-4284
Preprint. Discussion started: 15 September 2026

3.4 Temperature downscaling and precipitation analysis

The native spatial resolution of ERA5 is 0.25°× 0.25°(approximately 25–30 km), which provides only a coarse representation of meteorological conditions over mountain glaciers. Furthermore, ERA5 air temperature is reported at 2 m above the model surface, whose elevation often differs substantially from the glacier surface elevation. Individual ERA5 grid cells frequently encompass a wide range of topographic conditions, including glacierized terrain, mountain slopes, and low-elevation valleys. Consequently, the native ERA5 temperature fields do not adequately represent the strong altitudinal gradients present across glacier surfaces, making temperature downscaling necessary.

Hourly ERA5 reanalysis data for near-surface air temperature and total precipitation were used to quantify glacier-wide solid precipitation. ERA5 grid cells overlapping each glacier were processed individually to preserve spatial variability. Within each grid cell, a high-resolution reference digital elevation model (NASADEM) was masked using glacier outlines to extract only glacier-covered terrain. Elevation distributions were then represented by 100 m elevation bands, for which fractional glacier area was derived. Air temperature was downscaled from the ERA5 grid elevation to each elevation band employing a constant lapse rate of -6.5 °C per km, specified for the definition of standard atmosphere by International Civil Aviation Organization (1993). Precipitation was assumed to be spatially uniform within each ERA5 grid cell and was classified into solid and liquid components using a linear transition between 0 and 2 °C, representing a simplified temperature-threshold approach commonly applied in glacier and hydrological studies (e.g., Tobin et al., 2012; Bormann et al., 2014). Solid precipitation was computed for each elevation band and weighted by its fractional area, yielding a grid-cell-integrated estimate of glacier-wide snowfall. Time series from all contributing ERA5 grid cells were subsequently aggregated to obtain total glacier precipitation. Monthly and annual totals were derived, and precipitation characteristics were analysed over predefined multi-year periods.

4 Results and Discussion

4.1 Spatial variability of mass balance

Before analysing glacier-specific elevation changes, we first computed a map of elevation change patterns for the entire study region over the full observation period from 2000 to 2026 (Figure 3 a)). The region shows a strong melt signal of up to -6 m/yr, mostly observable on a few large outlet glaciers located around 44.5°S and 72.5°W. The largest glacier complex in this area corresponds to the first study site, the Queulat GC. In contrast to the Queulat GC, Melimoyu shows only limited signs of mass loss, with weak elevation lowering, restricted to small outlet glaciers surrounding the central accumulation area.

Hypsometric analysis (Figure 3 b)) reveals significant mass loss at lower elevations, while higher elevations (approximately 1900–2200 m a.s.l.) remain close to balance. The resulting total GMB of all glaciers in the study region amounts to approximately -0.67 m ± 0.27 m w.e./yr. This value is slightly more negative than the estimate of -0.57 ± 0.22 m w.e./yr reported for the northern Patagonia region by Dussaillant et al. (2019), yet less negative than the Southern Andes-wide average of -0.93 ± 0.22 m w.e./yr reported by The GlaMBIE Team et al. (2025). These differences can be attributed to several factors. First, the spatial extent of the respective studies differs substantially. Regional estimates from Dussaillant et al. (2019) and the GlaMBIE

https://doi.org/10.5194/egusphere-2026-4284
Preprint. Discussion started: 15 September 2026

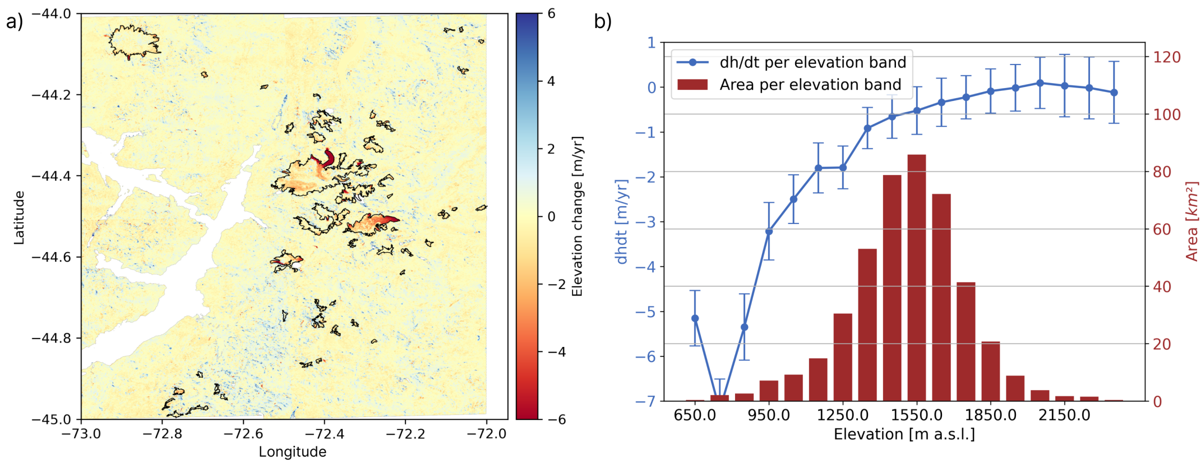

Figure 3. Elevation change rates (2000-2026) in test region a) and elevation binned average elevation changes of glacierized terrain b). The bars in sub-figure b) represent the uncertainties on elevation change ($\sigma_{dh,\mathrm{bin}}$) discussed in Section 3.3

Table 1. Elevation change and glacier mass balance (GMB) for different periods for the Queulat GC and stratovolcano Melimoyu.

Period	Queulat		Melimoyu	
	Avg dh/dt (m/yr)	GMB (m w.e./yr)	Avg dh/dt (m/yr)	GMB (m w.e./yr)
2000–2010	-0.28 ± 0.90	-0.23 ± 0.39	$+1.10 \pm 0.87$	$+0.95 \pm 0.37$
2011–2015	-0.31 ± 0.61	-0.26 ± 0.30	$+0.80 \pm 0.71$	$+0.69 \pm 0.23$
2016–2020	-0.54 ± 0.55	-0.45 ± 0.24	-0.16 ± 0.44	-0.14 ± 0.23
2021–2026	-0.75 ± 0.45	-0.63 ± 0.19	-0.17 ± 0.33	-0.14 ± 0.20

synthesis The GlaMBIE Team et al. (2025) include large icefields and a broader range of glacier types, while the present study focuses on a more limited subregion dominated by outlet glaciers and smaller GCs. Such differences in glacier geometry and hypsometry can strongly influence area-averaged mass balance. Second, discrepancies in temporal coverage likely contribute to the observed differences. Dussaillant et al. (2019) analyses the period 2000–2017, whereas the present study extends to 2026. As shown in the following sections, glacier mass loss in the study region has accelerated in recent years, leading to more negative mass balance estimates over the long term.

4.2 Glacier-scale differences and hypsometric control

Glacier-wide mass balance and average elevation change were computed for the periods 2000–2010, 2011–2015, 2016–2020, and 2021–2026. The results are summarised in Table 1. A pronounced difference is observed between the two GCs: Queulat GC exhibits consistently negative mass balances throughout the study period, with values becoming progressively more negative

https://doi.org/10.5194/egusphere-2026-4284
Preprint. Discussion started: 15 September 2026

from an initial -0.23 ± 0.39 m w.e./yr to -0.63 ± 0.19 m w.e./yr in the last 5 years. This evolution indicates a clear acceleration of mass loss over time.

In contrast, the stratovolcano Melimoyu shows strongly positive mass balance in the early period (+0.95 ± 0.37 m w.e./ yr for 2000–2010), followed by a steady decline towards near-zero and eventually slightly negative values (-0.14 ± 0.20 m w.e./yr for 2021–2026). This transition from accumulation to mass loss suggests a delayed response to climatic forcing compared to the Queulat GC.

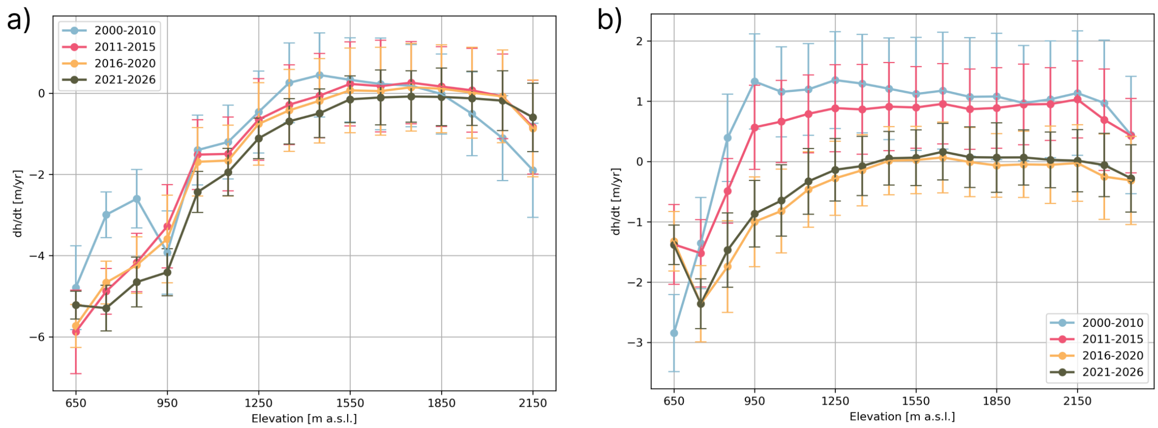

Figure 4. Elevation band averaged elevation changes for different time periods in a) Queulat GC and b) stratovolcano Melimoyu. The error bars represent the uncertainties on elevation change ($\sigma_{dh,\mathrm{bin}}$) discussed in Section 3.3

It should be noted that the positive mass balances may be somewhat overestimated because elevation gains in the accumulation area are likely associated with snow and firn, which generally have lower densities than the adopted density conversion factor of $850 \pm 60 kg/m^3$. However, it is recommended to apply this value for both positive and negative geodetic volume changes, as glacier-wide elevation changes typically reflect a combination of snow, firn, and ice rather than a single material. Therefore, in the absence of detailed information on firn conditions and densification processes, the use of a density conversion factor of $850 \pm 60 kg/m^3$ remains the recommended approach (Huss, 2013; Zemp et al., 2013).

Large errors observed in the earlier period 2000-2010 mainly stem from random errors (Section 3.3, equation 4), specifically uncertainty on the elevation change rate component σ_{dh} and systematic errors (Section 3.3, equation 5). During this period, fewer DEMs are available, resulting in two slightly different estimates of the half-periods used in equation 5. Large systematic errors under limited DEM availability are also observed in other studies (Brun et al., 2017).

Additionally, uncertainties in elevation change and, consequently, in glacier mass balance for earlier periods (2000-2010 and 2011-2015) are systematically higher than those for more recent periods (2016-2020 and 2021-2026). Visual inspection of the resulting dh/dt maps indicates increased noise levels and a greater number of data voids in maps generated for the first two temporal periods. Such behaviour has not been widely reported in studies using self-processed DEMs generated with tools

https://doi.org/10.5194/egusphere-2026-4284
Preprint. Discussion started: 15 September 2026

such as the Ames Stereo Pipeline (Beyer et al., 2018) or MicMac (Rupnik et al., 2017). While a detailed investigation of the underlying causes is beyond the scope of this study, potential explanations may include differences in data availability for raw and pre-processed DEMs or DEM processing strategies. This discrepancy demands further investigation in future work.

The observed differences in mass balance between the two glacier systems can primarily be attributed to differences in glacier geometry and hypsometry. The Queulat GC has a larger proportion of its area at low elevations (below 1000 m a.s.l.), making it more sensitive to temperature-driven melt processes compared to Melimoyu, which is characterised by a larger proportion of its area at mid to high elevations, where conditions remain closer to the equilibrium line altitude (ELA) during most of the study period.

This contrast is reflected in the elevation-dependent elevation change patterns (Figure 4). For Queulat GC (Figure 4, a), strong elevation lowering is observed at low elevations, with rates exceeding -5 m/yr in the lowest elevation bands. With increasing elevation, the magnitude of elevation change gradually decreases, approaching near-neutral or slightly positive values in the highest bands for earlier periods. Over time, the hypsometric curves show a systematic downward shift, indicating an overall intensification of mass loss. In the most recent period (2021–2026), negative elevation rates are present for all elevation bands, indicating an upward migration of the ELA.

At higher elevations of Queulat GC (above 1800 m a.s.l.), a reduction in the magnitude of elevation change over time is observed. This behaviour can be attributed to the geomorphological setting of the glacier, where ice at these elevations is largely confined to steep and narrow mountain ridges (Figure 5a). In many locations, glacier ice has already been substantially reduced or replaced by exposed bedrock, resulting in smaller apparent elevation changes and a reduced sensitivity to further melt.

Conversely, the Melimoyu (Figure 4, b) exhibits a remarkably different behaviour. During the early period (2000–2010), positive elevation changes dominate at mid- and high elevations, in some cases exceeding +1 m/yr. These positive rates diminish over time, and by the most recent period, elevation changes at most elevations are close to zero or slightly negative. This transition indicates a shift from accumulation-dominated conditions to near-balanced or slightly negative mass balance, consistent with the results calculated for all glaciers in the region as discussed above.

The contrasting behaviour of Queulat and Melimoyu demonstrates that glacier geometry can strongly influence both the magnitude and spatial distribution of elevation change. Despite their close proximity and exposure to broadly similar climatic forcing, the two glacier systems exhibit substantially different thinning patterns. This finding demonstrates that regional-scale geodetic mass-balance products, while invaluable for quantifying regional trends, may overlook important glacier-scale variability in glacier response to climate change.

The spatial distribution of elevation bands and associated elevation changes (Figure 5) provides further insight into the controlling mechanisms. For Queulat GC (Figure 5 a), c)), low elevations correspond to extensive outlet glacier tongues, which experience the strongest mass loss. Higher elevations are limited to narrow, steep ridges, where glacier area has already been substantially reduced and elevation changes are comparatively small. In contrast, Melimoyu (Figure 5 b), d)) exhibits a more radially symmetric hypsometry, characterised by a broad elevation distribution and a large, relatively flat high-elevation plateau. This geometry favours sustained accumulation at high elevations during the early period. However, the extensive high-

https://doi.org/10.5194/egusphere-2026-4284
Preprint. Discussion started: 15 September 2026

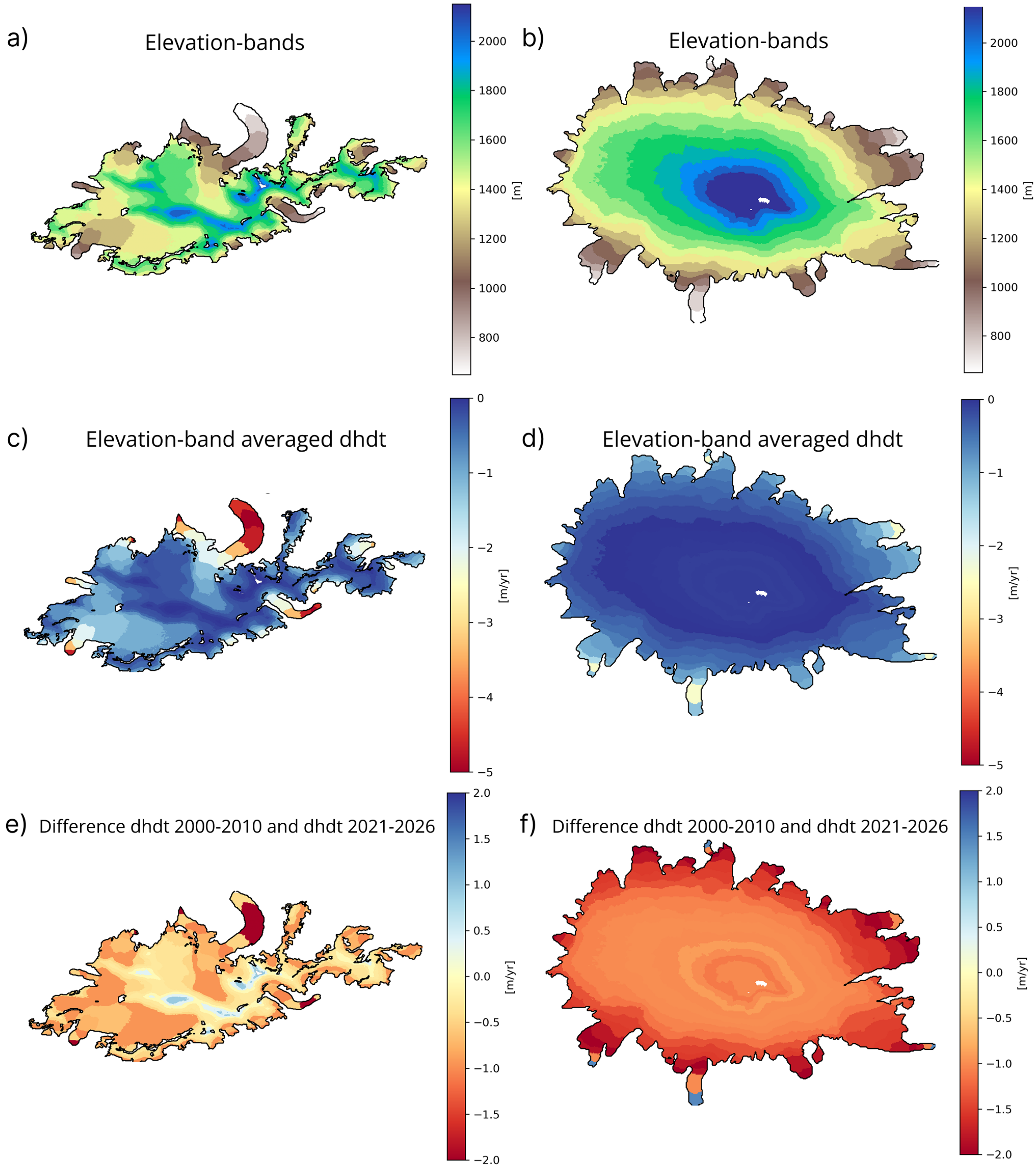

Figure 5. Spatial distribution of elevation bands in a) Queulat GC and b) stratovolcano Melimoyu, average elevation changes per elevation band over the full time period 2000-2026 in c) Queulat GC and d) stratovolcano Melimoyu and changes in elevation change rates computed between 2000-2010 period and 2021-2026 in e) Queulat GC and f) stratovolcano Melimoyu

https://doi.org/10.5194/egusphere-2026-4284
Preprint. Discussion started: 15 September 2026

elevation plateau also means that a large glacier area is affected once negative mass-balance conditions develop, contributing to the increasing elevation loss observed in recent periods.

Temporal changes in elevation change rates (Figure 5 e), f)), computed from the dh/dt differences of the first and last analysed periods, further highlight the contrasting glacier responses. Melimoyu shows a broadly coherent increase in mass loss across most elevation bands, while the lowest elevations exhibit reduced thinning rates, likely due to glacier retreat and the progressive disappearance of low-elevation ice. Queulat GC displays a more heterogeneous pattern. Mid-elevation zones (1000–1500 m a.s.l.), corresponding to the main part of outlet glaciers, show the strongest increase in thinning, whereas the areas with the highest elevations (above 1800 m a.s.l.) retain similar mass loss rates. The lowest elevation bands exhibit a reduced rate of elevation loss in recent years, again reflecting terminus retreat beyond the reference outlines.

Overall, these results suggest that hypsometry and glacier geometry exert a strong influence on glacier response. Although the ERA5 analysis presented in Section 4.4 reveals slightly stronger warming and snowfall reduction over the Queulat GC, the climatic differences between the two study sites are substantially smaller than the observed differences in mass balance. This indicates that glacier geometry and elevation distribution play a major role in shaping their contrasting mass-balance trajectories.

The results further highlight the role of glacier hypsometry in controlling glacier sensitivity to climatic forcing. Queulat contains a large proportion of its area within a relatively narrow elevation range, whereas Melimoyu exhibits a broader elevation distribution and retains a greater proportion of glacier area at higher elevations. Consequently, relatively small shifts in equilibrium-line altitude may affect a larger fraction of the Queulat glacier complex simultaneously, while accumulation areas may persist over a wider range of climatic conditions on Melimoyu.

4.3 Comparison with existing datasets

To assess the robustness of our elevation change estimates, we compared our results with the glacier elevation change dataset of Hugonnet et al. (2021), which provides a timeseries of annual elevation change rates for individual glaciers at the RGI 6 level for the period 2000–2016. In order to ensure comparability, we extracted time series of elevation change for all glaciers contributing to the two study sites and aggregated these values spatially to match the extent of the GCs analysed in this study.

The comparison summarised in Table 2 shows that our estimates generally exhibit less negative magnitudes of elevation change compared to the Hugonnet et al. (2021) dataset. For the Queulat GC, the differences are relatively small, and our values consistently lie within the uncertainty ranges reported by Hugonnet et al. (2021). This indicates a good overall agreement between the two approaches. In contrast, larger discrepancies are observed for the Melimoyu, particularly in the earlier periods, where our dataset suggests substantially stronger positive elevation changes.

The differences in computed dhdt can be attributed to several factors. First, methodological differences between the two studies play an important role. While the Hugonnet dataset is based on a multi-source DEM time series with spatial filtering and gap-filling approaches optimised for large-scale analysis, our study utilises a higher spatial resolution DEM dataset (30 m), which may better capture small-scale elevation variability but can also increase sensitivity to data noise. In contrast, the coarser

https://doi.org/10.5194/egusphere-2026-4284
Preprint. Discussion started: 15 September 2026

Table 2. Comparison of elevation change rates (dh/dt) between this study and Hugonnet et al. (2021). for the Queulat GC and the stratovolcano Melimoyu.

Period	Queulat GC (Hugonnet et al. (2021)) (m/yr)	Queulat GC (this study) (m/yr)	Volcano (Hugonnet et al. (2021)) (m/yr)	Volcano (this study) (m/yr)
2000–2010	-0.47 ± 0.74	-0.28 ± 0.90	$+0.10 \pm 0.58$	$+1.10 \pm 0.87$
2010–2015	-0.80 ± 0.64	-0.31 ± 0.61	-0.34 ± 0.54	$+0.80 \pm 0.71$
2015–2020	-0.95 ± 0.60	-0.54 ± 0.55	-0.62 ± 0.55	-0.16 ± 0.33

spatial resolution (100 m) used in the Hugonnet dataset may result in a smoothing of elevation changes, particularly in areas with complex topography.

Additional differences arise from the use of updated glacier outlines in this study (RGI 7 vs. RGI 6). The comparison showed substantial differences for the geometries of Queulat GC. In the case of the Stratovolcano GC, several glacier outlets in RGI 6 appear spatially displaced relative to their positions in RGI 7. Furthermore, the total area of the Queulat GC increases from 93.6 km^2 in RGI 6 to 102.6 km^2 in RGI 7, indicating a considerable revision of glacier extent. In contrast, for stratovolcano Melimoyu, the difference is less pronounced, with areas of 57.4 km^2 (RGI 6) and 55.8 km^2 (RGI 7).

Overall, despite these differences, the agreement between our results and the Hugonnet dataset is generally good for the Queulat GC and remains within uncertainty bounds. The larger discrepancies observed for the Melimoyu highlight the sensitivity of elevation change estimates to data quality, glacier geometry, and methodological choices.

4.4 Climatic controls on local mass balance changes

To assess whether differences in climatic forcing could explain the contrasting glacier behaviour of the two test sites, trends in near-surface air temperature and precipitation were derived from ERA5 reanalysis data. In particular, we analyse changes in summer temperature and annual solid precipitation (snowfall), which directly influence ablation and accumulation processes.

Summer temperature trends in Figure 6 indicate a consistent warming across the study region over the period 2000–2026. The magnitude of warming differs slightly between the two sites, with the Queulat GC exhibiting a stronger increase of +0.45°C per decade compared to the Melimoyu with +0.3°C per decade. Although the difference in temperature trends is relatively small, the higher sensitivity of Queulat GC to temperature changes, as indicated by its low-elevation-dominated hypsometry, likely amplifies the impact of this warming on glacier mass balance.

ERA5-derived precipitation shows only minor differences between the two study areas (Figure 7 a), b)). Both sites exhibit similar magnitudes of annual snowfall, with Queulat GC reaching values of up to approximately 11 000 mm w.e./yr during the early part of the observation period and decreasing to around 9 500 mm w.e./yr in recent years. The Melimoyu shows lower overall snowfall, ranging from approximately 7 000 mm w.e./yr to 6 500 mm w.e./yr over the same period. However, the relative changes in precipitation between the two sites remain small compared to the pronounced differences in mass balance.

https://doi.org/10.5194/egusphere-2026-4284
Preprint. Discussion started: 15 September 2026

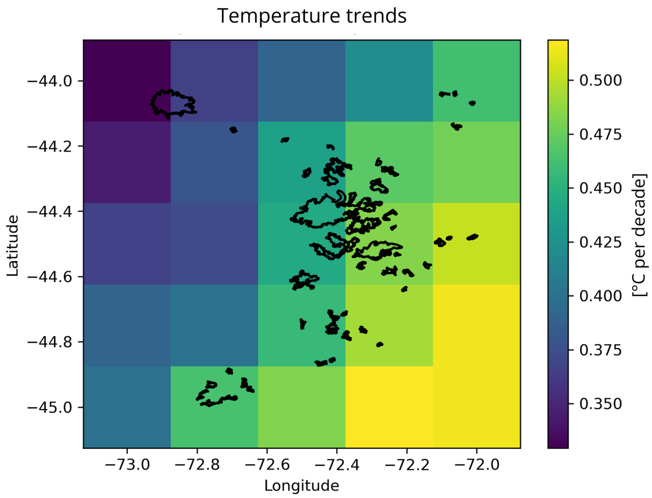

Figure 6. Temperature trends for the study region derived from ERA5 data

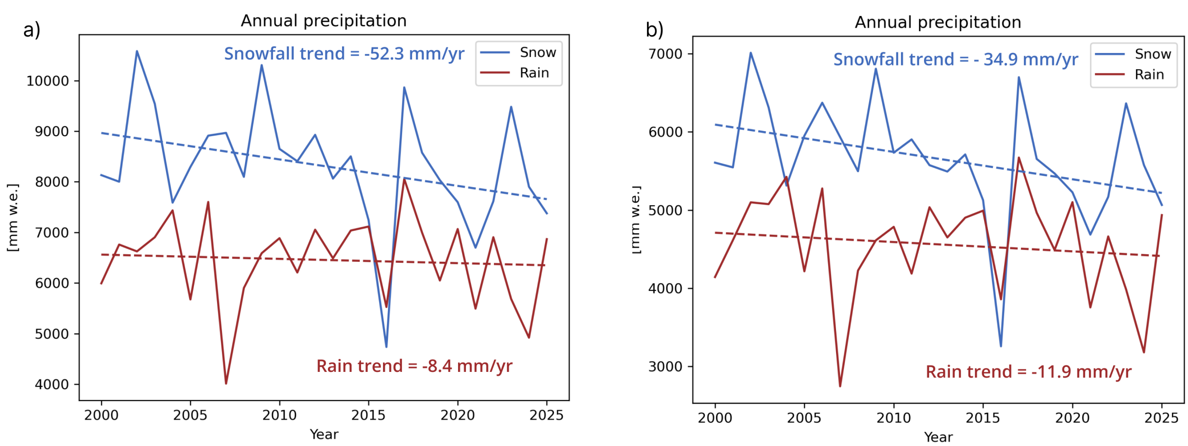

Figure 7. Annual solid (snowfall) and liquid (rain) precipitation over a) Queulat GC and b) stratovolcano Melimoyu

It should be noted that ERA5 has a coarse spatial resolution (25 km), which limits its ability to resolve small-scale precipitation gradients in complex topography. Given the relatively short distance between the two glacier systems (50 km), ERA5 likely smooths spatial differences in precipitation, which may contribute to the limited contrast observed in the reanalysis data.

A consistent feature at both sites is a declining trend in solid precipitation, accompanied by increasing air temperatures. This suggests a shift in precipitation phase from snow to rain, particularly at elevations close to the ELA. Such a phase shift reduces effective accumulation even when total precipitation remains relatively stable, as evidenced by the acceleration of glacier surface lowering observed in this study (Table 1).

https://doi.org/10.5194/egusphere-2026-4284
Preprint. Discussion started: 15 September 2026

Overall, the ERA5 data indicate a regional trend towards warmer conditions and reduced snowfall, rather than substantial differences in precipitation input between the two glacier systems. Consequently, the contrasting glacier behaviour observed in this study is most plausibly explained by differences in glacier geometry and hypsometry, which modulate each system's sensitivity to similar climatic forcing.

5 Conclusions

This study examined glacier elevation changes and glacier mass balance using DEM differencing for two neighbouring glacier systems with contrasting geometry in the Southern Andes. The results show clear differences in glacier response despite exposure to broadly similar climatic conditions, pointing out the critical role of glacier-specific characteristics.

The Queulat GC displays persistent and accelerating mass loss over the study period, with the strongest thinning observed at low elevations where extensive outlet glacier tongues dominate. This pattern illustrates the high sensitivity of low-elevation-dominated glacier systems to temperature-driven ablation.

In contrast, the stratovolcano Melimoyu shows near-neutral to slightly negative mass balance over much of the study period, with only a recent shift towards increasing mass loss. Although thinning is also observed at lower elevations, the overall response remains more moderate. This delayed and reduced sensitivity can be attributed to the wider elevation distribution of the glacier system, which maintains a larger proportion of glacier area at high elevations.

The comparison between the two glacier systems indicates that glacier geometry and hypsometry exert a first-order control on glacier response to climatic forcing. While ERA5 data indicate similar warming trends and decreasing snowfall at both sites, differences in glacier elevation distributions significantly influence the resulting mass-balance trajectories. These findings emphasise that glacier-scale heterogeneity can lead to divergent responses that are not captured by regional-scale averages. In northern Patagonia, where different types of glaciers and volcanic ice caps coexist within a relatively confined region, glacier-specific characteristics therefore need to be considered when interpreting present-day glacier change and projecting future glacier evolution.

Furthermore, our results illustrate the value of ASTER-derived DEM differencing for resolving elevation-change patterns across individual elevation bands. While glacier-wide mass-balance estimates provide an important measure of overall glacier change, the elevation-dependent analysis shows substantial spatial variability in thinning and apparent accumulation that would otherwise stay concealed. Such information can improve the interpretation of glacier response to climatic forcing and provide additional insight beyond glacier- or regionally averaged mass-balance estimates.

Observations of increased noise levels, data voids, and higher uncertainties in earlier time periods point to temporal inconsistencies in AST14DEM quality and availability. These effects may influence derived elevation-change rates and mass-balance estimates, and are not widely discussed in studies based on self-processed DEMs generated using tools such as the Ames Stereo Pipeline or MicMac. A systematic comparison between ASTER standard products and common pre-processing algorithms would therefore be valuable to better understand potential biases, differences in signal detectability, and their implications for long-term glacier monitoring.

https://doi.org/10.5194/egusphere-2026-4284
Preprint. Discussion started: 15 September 2026

Overall, the results demonstrate that glacier geometry and hypsometry are key controls on glacier sensitivity to climate change in northern Patagonia. Future projections of glacier evolution, runoff generation, and water-resource availability would therefore benefit from a more explicit representation of elevation distributions and elevation-dependent mass balance. Accounting for these controls may reduce uncertainties in glacier-scale projections and improve the interpretation of regional glacier-change estimates across the Southern Andes.

Data availability. The dh/dt maps of study sites together with statistical information on elevation bins for time periods 2000-2026, 2000-2010, 2011-2015, 2016-2020 and 2021-2026 are available upon request.

Author contributions. RP, CM, MU and AW conceptualised the research and designed the study. MU performed formal analysis with supervision from CM, RP, MR and AW. MU prepared the draft of this paper. All the co-authors contributed to the paper editing.

Competing interests. The contact author has declared that none of the authors has any competing interests.

References

GLOSSARY OF GLACIER MASS BALANCE AND RELATED TERMS. J.G. Cogley, R. Hock, L.A. Rasmussen, A.A. Arendt, A. Bauder, R.J. Braithwaite, P. Jansson, G. Kaser, M. Möller, L. Nicholson, and M. Zemp. 2011. Paris: UNESCO-IHP (IHP-VII Technical documents in hydrology 86, IACS contribution 2) volume=48, DOI=10.1017/S0032247411000805, number=4, journal=Polar Record, author=Pope, Allen, year=2012, pages=e15.

Abrams, M.: The Advanced Spaceborne Thermal Emission and Reflection Radiometer (ASTER): Data products for the high spatial resolution imager on NASA's Terra platform, International Journal of Remote Sensing, 21, 847–859, https://doi.org/10.1080/014311600210326, 2000.

Berthier, E., Cabot, V., Vincent, C., and Six, D.: Decadal Region-Wide and Glacier-Wide Mass Balances Derived from Multi-Temporal ASTER Satellite Digital Elevation Models. Validation over the Mont-Blanc Area, Frontiers in Earth Science, 4, https://doi.org/10.3389/feart.2016.00063, 2016.

Beyer, R. A., Alexandrov, O., and McMichael, S.: The Ames Stereo Pipeline: NASA's Open Source Software for Deriving and Processing Terrain Data, Earth and Space Science, 5, 537–548, https://doi.org/https://doi.org/10.1029/2018EA000409, 2018.

Bormann, K. J., Evans, J. P., and McCabe, M. F.: Constraining snowmelt in a temperature-index model using simulated snow densities, Journal of Hydrology, 517, 652–667, https://doi.org/https://doi.org/10.1016/j.jhydrol.2014.05.073, 2014.

Braun, M. H., Malz, P., Sommer, C., Farías-Barahona, D., Sauter, T., Casassa, G., Soruco, A., Skvarca, P., and Seehaus, T. C.: Constraining glacier elevation and mass changes in South America, Nature Climate Change, 9, 130–136, https://doi.org/10.1038/s41558-018-0375-7, 2019.

Brun, F., Berthier, E., Wagnon, P., Kääb, A., and Treichler, D.: A spatially resolved estimate of High Mountain Asia glacier mass balances from 2000 to 2016, Nature Geoscience, 10, 668–673, https://doi.org/10.1038/ngeo2999, 2017.

Buckley, S. M., Agram, P. S., Belz, J. E., Crippen, R. E., Gurrola, E. M., Hensley, S., Kobrick, M., Lavallev, M., Martin, J. M., Neumann, M., Nguyen, Q. D., Rosen, P. A., Shimada, J. G., Simard, M., and Tung, W. W.: NASADEM, https://www.earthdata.nasa.gov/data/catalog/lpcloud-nasadem-hgt-001#toc-user-s-guide, 2025.

Chen, J., Tapley, B., and Wilson, C.: Alaskan mountain glacial melting observed by satellite gravimetry, Earth and Planetary Science Letters, 248, 368–378, https://doi.org/10.1016/j.epsl.2006.05.039, 2006.

Copernicus Climate Change Service, C. D. S.: ERA5 hourly data on single levels from 1940 to present. Copernicus Climate Change Service (C3S) Climate Data Store (CDS), https://doi.org/10.24381/cds.adbb2d47, (Accessed on May 10, 2026), 2023.

Dussaillant, I., Berthier, E., Brun, F., Masiokas, M., Hugonnet, R., Favier, V., Rabatel, A., Pitte, P., and Ruiz, L.: Two decades of glacier mass loss along the Andes, Nature Geoscience, 12, 802–808, https://doi.org/10.1038/s41561-019-0432-5, 2019.

Fischer, M., Huss, M., and Hoelzle, M.: Surface elevation and mass changes of all Swiss glaciers 1980–2010, The Cryosphere, 9, 525–540, https://doi.org/10.5194/tc-9-525-2015, 2015.

Fujisada, H., Bailey, G., Kelly, G., Hara, S., and Abrams, M.: ASTER DEM performance, IEEE Transactions on Geoscience and Remote Sensing, 43, 2707–2714, https://doi.org/10.1109/TGRS.2005.847924, 2005.

Garreaud, R. D.: The Andes climate and weather, Advances in Geosciences, 22, 3–11, https://doi.org/10.5194/adgeo-22-3-2009, 2009.

Garreaud, R. D., Vuille, M., Compagnucci, R., and Marengo, J.: Present-day South American climate, Palaeogeography, Palaeoclimatology, Palaeoecology, 281, 180–195, https://doi.org/https://doi.org/10.1016/j.palaeo.2007.10.032, 2009.

https://doi.org/10.5194/egusphere-2026-4284
Preprint. Discussion started: 15 September 2026

Hersbach, H., Bell, B., Berrisford, P., Hirahara, S., Horányi, A., Muñoz-Sabater, J., Nicolas, J., Peubey, C., Radu, R., Schepers, D., Simmons, A., Soci, C., Abdalla, S., Abellan, X., Balsamo, G., Bechtold, P., Biavati, G., Bidlot, J., Bonavita, M., De Chiara, G., Dahlgren, P., Dee, D., Diamantakis, M., Dragani, R., Flemming, J., Forbes, R., Fuentes, M., Geer, A., Haimberger, L., Healy, S., Hogan, R. J., Hólm, E., Janisková, M., Keeley, S., Laloyaux, P., Lopez, P., Lupu, C., Radnoti, G., de Rosnay, P., Rozum, I., Vamborg, F., Villaume, S., and Thépaut, J.-N.: The ERA5 global reanalysis, Quarterly Journal of the Royal Meteorological Society, 146, 1999–2049, https://doi.org/10.1002/qj.3803, 2020.

Hock, R., Bliss, A., Marzeion, B., Giesen, R. H., Hirabayashi, Y., Huss, M., Radić, V., and Slangen, A. B. A.: GlacierMIP – A model intercomparison of global-scale glacier mass-balance models and projections, Journal of Glaciology, 65, 453–467, https://doi.org/10.1017/jog.2019.22, 2019.

Hugonnet, R., McNabb, R., Berthier, E., Menounos, B., Nuth, C., Girod, L., Farinotti, D., Huss, M., Dussaillant, I., Brun, F., and Kääb, A.: Accelerated global glacier mass loss in the early twenty-first century, Nature, 592, 726–731, https://doi.org/10.1038/s41586-021-03436-z, 2021.

Huss, M.: Extrapolating glacier mass balance to the mountain-range scale: the European Alps 1900–2100, The Cryosphere, 6, 713–727, https://doi.org/10.5194/tc-6-713-2012, 2012.

Huss, M.: Density assumptions for converting geodetic glacier volume change to mass change, The Cryosphere, 7, 877–887, https://doi.org/10.5194/tc-7-877-2013, 2013.

Huss, M. and Hock, R.: A new model for global glacier change and sea-level rise, Frontiers in Earth Science, Volume 3 - 2015, https://doi.org/10.3389/feart.2015.00054, 2015.

International Civil Aviation Organization: Manual of the ICAO Standard Atmosphere: Extended to 80 Kilometres (262 500 Feet), Doc (International Civil Aviation Organization), International Civil Aviation Organization, https://books.google.de/books?id=4RgKxAEACAAJ, 1993.

Kääb, A., Berthier, E., Nuth, C., Gardelle, J., and Arnaud, Y.: Contrasting patterns of early twenty-first-century glacier mass change in the Himalayas, Nature, 488(7412), 495–498, https://doi.org/doi:10.1038/nature11324, 2012.

Lehner, B., Anand, M., Fluet-Chouinard, E., Tan, F., Aires, F., Allen, G. H., Bousquet, P., Canadell, J. G., Davidson, N., Ding, M., Finlayson, C. M., Gumbricht, T., Hilarides, L., Hugelius, G., Jackson, R. B., Korver, M. C., Liu, L., McIntyre, P. B., Nagy, S., Olefeldt, D., Pavelsky, T. M., Pekel, J.-F., Poulter, B., Prigent, C., Wang, J., Worthington, T. A., Yamazaki, D., Zhang, X., and Thieme, M.: Mapping the world's inland surface waters: an upgrade to the Global Lakes and Wetlands Database (GLWD v2), Earth System Science Data, 17, 2277–2329, https://doi.org/10.5194/essd-17-2277-2025, 2025.

Malz, P., Meier, W., Casassa, G., Jaña, R., Skvarca, P., and Braun, M. H.: Elevation and Mass Changes of the Southern Patagonia Icefield Derived from TanDEM-X and SRTM Data, Remote Sensing, 10, https://doi.org/10.3390/rs10020188, 2018.

McDonnell, M., Rupper, S., and Forster, R.: Quantifying Geodetic Mass Balance of the Northern and Southern Patagonian Icefields Since 1976, Frontiers in Earth Science, Volume 10 - 2022, https://doi.org/10.3389/feart.2022.813574, 2022.

Moholdt, G., Nuth, C., Hagen, J. O., and Kohler, J.: Recent elevation changes of Svalbard glaciers derived from ICESat laser altimetry, Remote Sensing of Environment, 114, 2756–2767, https://doi.org/10.1016/j.rse.2010.06.008, 2010.

NASA, METI, AIST, Japan Spacesystems, and U.S./Japan ASTER Science Team: ASTER Digital Elevation Model [Data set], https://doi.org/10.5067/ASTER/AST14DEM.004, 2025.

NASA Earthdata: Shuttle Radar Topography Mission (SRTM), https://www.earthdata.nasa.gov/data/instruments/srtm.

NASA JPL: Advanced Spaceborne Thermal Emission and Reflection Radiometer (ASTER), https://asterweb.jpl.nasa.gov/index.asp, 2004.

https://doi.org/10.5194/egusphere-2026-4284
Preprint. Discussion started: 15 September 2026

NASA JPL: NASADEM Merged DEM Global 1 arc second V001, https://doi.org/10.5067/MEASURES/NASADEM/NASADEM_HGT.001, 2020.

Nuth, C. and Kääb, A.: Co-registration and bias corrections of satellite elevation data sets for quantifying glacier thickness change, The Cryosphere, 5, 271–290, https://doi.org/10.5194/tc-5-271-2011, 2011.

Paul, F.: Revealing glacier flow and surge dynamics from animated satellite image sequences: examples from the Karakoram, The Cryosphere, 9, 2201–2214, https://doi.org/10.5194/tc-9-2201-2015, 2015.

RGI 7.0 Consortium: Randolph Glacier Inventory - A Dataset of Global Glacier Outlines, Version 7.0, https://doi.org/doi:10.5067/f6jmovy5navz, 2023.

Rivera, A. and Bown, F.: Recent glacier variations on active ice capped volcanoes in the Southern Volcanic Zone (37°–46°S), Chilean Andes, Journal of South American Earth Sciences, 45, 345–356, https://doi.org/https://doi.org/10.1016/j.jsames.2013.02.004, 2013.

Rupnik, E., Daakir, M., and Pierrot Deseilligny, M.: MicMac – a free, open-source solution for photogrammetry, Open Geospatial Data, Software and Standards, 2, 14, https://doi.org/10.1186/s40965-017-0027-2, 2017.

The GlaMBIE Team, Zemp, M., Jakob, L., Dussaillant, I., Nussbaumer, S. U., Gourmelen, N., Dubber, S., A, G., Abdullahi, S., Andreassen, L. M., Berthier, E., Bhattacharya, A., Blazquez, A., Boehm Vock, L. F., Bolch, T., Box, J., Braun, M. H., Brun, F., Cicero, E., Colgan, W., Eckert, N., Farinotti, D., Florentine, C., Floricioiu, D., Gardner, A., Harig, C., Hassan, J., Hugonnet, R., Huss, M., Jóhannesson, T., Liang, C.-C. A., Ke, C.-Q., Khan, S. A., King, O., Kneib, M., Krieger, L., Maussion, F., Mattea, E., McNabb, R., Menounos, B., Miles, E., Moholdt, G., Nilsson, J., Pálsson, F., Pfeffer, J., Piermattei, L., Plummer, S., Richter, A., Sasgen, I., Schuster, L., Seehaus, T., Shen, X., Sommer, C., Sutterley, T., Treichler, D., Velicogna, I., Wouters, B., Zekollari, H., and Zheng, W.: Community estimate of global glacier mass changes from 2000 to 2023, Nature, https://doi.org/10.1038/s41586-024-08545-z, 2025.

Tobin, C., Rinaldo, A., and Schaefli, B.: Snowfall Limit Forecasts and Hydrological Modeling, Journal of Hydrometeorology, 13, 1507 – 1519, https://doi.org/10.1175/JHM-D-11-0147.1, 2012.

Van Wyk de Vries, M., Romero, M., Penprase, S. B., Ng, G.-H. C., and Wickert, A. D.: Increasing rate of 21st century volume loss of the Patagonian Icefields measured from proglacial river discharge, Journal of Glaciology, 69, 1187–1202, https://doi.org/10.1017/jog.2023.9, 2023.

Wang, D. and Kääb, A.: Modeling Glacier Elevation Change from DEM Time Series, Remote Sensing, 7, 10 117–10 142, https://doi.org/10.3390/rs70810117, 2015.

Willis, M. J., Melkonian, A. K., Pritchard, M. E., and Ramage, J. M.: Ice loss rates at the Northern Patagonian Icefield derived using a decade of satellite remote sensing, Remote Sensing of Environment, 117, 184–198, https://doi.org/https://doi.org/10.1016/j.rse.2011.09.017, remote Sensing of Urban Environments, 2012a.

Willis, M. J., Melkonian, A. K., Pritchard, M. E., and Rivera, A.: Ice loss from the Southern Patagonian Ice Field, South America, between 2000 and 2012, Geophysical Research Letters, 39, 2012GL053 136, https://doi.org/10.1029/2012GL053136, 2012b.

Wouters, B., Gardner, A. S., and Moholdt, G.: Global Glacier Mass Loss During the GRACE Satellite Mission (2002-2016), Frontiers in Earth Science, 7, 96, https://doi.org/10.3389/feart.2019.00096, 2019.

xDEM contributors: xDEM, https://doi.org/10.5281/zenodo.19636034, 2026.

Zemp, M., Thibert, E., Huss, M., Stumm, D., Rolstad Denby, C., Nuth, C., Nussbaumer, S. U., Moholdt, G., Mercer, A., Mayer, C., Joerg, P. C., Jansson, P., Hynek, B., Fischer, A., Escher-Vetter, H., Elvehøy, H., and Andreassen, L. M.: Reanalysing glacier mass balance measurement series, The Cryosphere, 7, 1227–1245, https://doi.org/10.5194/tc-7-1227-2013, 2013.

https://doi.org/10.5194/egusphere-2026-4284
Preprint. Discussion started: 15 September 2026

Zemp, M., Huss, M., Thibert, E., Eckert, N., McNabb, R., Huber, J., Barandun, M., Machguth, H., Nussbaumer, S. U., Gärtner-Roer, I., Thomson, L., Paul, F., Maussion, F., Kutuzov, S., and Cogley, J. G.: Global glacier mass changes and their contributions to sea-level rise from 1961 to 2016, Nature, 568, 382–386, https://doi.org/10.1038/s41586-019-1071-0, 2019.

Zhang, M. and Gunturk, B. K.: Multiresolution Bilateral Filtering for Image Denoising, IEEE Transactions on Image Processing, 17, 2324–2333, https://doi.org/10.1109/TIP.2008.2006658, 2008.